Applied Physics Letters

RESEARCH ARTICLE | JULY 11 2023

Comprehensive excited state carrier dynamics of 2D selenium: One-photon and multi-photon absorption regimes

Sayan Prodhan ; Kamlesh Kumar Chauhan ; Tara Singha ; Manobina Karmakar ; Nikhilesh Maity ; Renjith Nadarajan ; Partha Kumbhakar ; Chandra Sekhar Tiwary ; Abhishek Kumar Singh ; Manikoth M. Shaijumon ; Prasanta Kumar Datta

Appl. Phys. Lett. 123, 021105 (2023)
https://doi.org/10.1063/5.0156843

AIP Publishing

Applied Physics Letters ARTICLE pubs.aip.org/aip/apl

Comprehensive excited state carrier dynamics of 2D selenium: One-photon and multi-photon absorption regimes

Cite as: Appl. Phys. Lett. **123**, 021105 (2023); doi: 10.1063/5.0156843
Submitted: 3 May 2023 · Accepted: 13 June 2023 ·
Published Online: 11 July 2023

Sayan Prodhan,[1] Kamlesh Kumar Chauhan,[2] Tara Singha,[1] Manobina Karmakar,[1,a)] Nikhilesh Maity,[3] Renjith Nadarajan,[4] Partha Kumbhakar,[5,b)] Chandra Sekhar Tiwary,[5] Abhishek Kumar Singh,[3] Manikoth M. Shaijumon,[4] and Prasanta Kumar Datta[1,c)]

AFFILIATIONS

[1]Department of Physics, Indian Institute of Technology (IIT) Kharagpur, Kharagpur 721302, India
[2]Department of Electrical Engineering, Indian Institute of Technology (IIT) Kharagpur, Kharagpur 721302, India
[3]Materials Research Centre, Indian Institute of Science, Bangalore 560012, India
[4]School of Physics, Indian Institute of Science Education and Research Thiruvananthapuram (IISER TVM), Maruthamala PO, Thiruvananthapuram, Kerala 695551, India
[5]Department of Metallurgical and Materials Engineering, Indian Institute of Technology Kharagpur, Kharagpur 721302, India

[a)]**Current address:** NanoScience Technology Center, University of Central Florida, Orlando, Florida 32826, USA.
[b)]**Current address:** Department of Physics and Electronics, CHRIST, Bangalore 560029, India.
[c)]**Author to whom correspondence should be addressed:** pkdatta@phy.iitkgp.ac.in

ABSTRACT

Semiconductors play a critical role in optoelectronic applications, and recent research has identified group-VI 2D semiconductors as promising materials for this purpose. Here, we report the comprehensive excited state carrier dynamics of bilayer, two-dimensional (2D) selenium (Se) in one-photon and multi-photon absorption regimes using transient reflection (TR) spectroscopy. Carrier lifetime obtained from TR measurement is used to theoretically predict the photo-responsivity for 2D Se photo-detectors operating in the one-photon-absorption regime. We also calculate a giant two-photon absorption cross section of 2.9×10^5 GM at 750 nm hinting possible application of 2D Se as a sub-bandgap photo-detector. The carrier recombination process is dominated by surface and sub-surface defect states in one- and multi-photon absorption regimes, respectively, resulting nearly one order increased carrier lifetime in a three-photon-absorption regime (1700 ps) compared to a one-photon-absorption regime (103 ps). Femtosecond Z-scan measurement shows saturation behavior for above bandgap excitation, further indicating the possibility of 2D Se as a saturable absorber material for passive Q-switching. Our study provides comprehensive insight into the excited state carrier dynamics of bilayer 2D Se and highlights its potential as a versatile material for various linear and non-linear optoelectronic applications.

Following the discovery of graphene,[1] two-dimensional (2D) materials have captured the spotlight in the research community due to the structural versatility and electronic properties affecting their physical and chemical properties.[2–4] Recently, group VI 2D semiconductors, specifically selenene and tellurene, are turning out to be promising materials having great potential applications in optoelectronics due to their simple composition, large carrier mobility, excellent environmental stability, and high photoconductivity.[5–9] Xing *et al.* have demonstrated a 2D Se-nanosheet-based optical modulation device, which allows for excellent ultrashort pulse generation of an optical communication band.[10] Sarma *et al.* have synthesized highly crystalline ultrathin 2D Se. They have studied the optical response of a photodetector fabricated using a bilayer selenene.[11]

Though various forms of selenium (Se) like square-selenene or any monoclinic forms (α-Se, β-Se, and γ-Se) are available, trigonal selenium (t-Se) dominates in optoelectronic applications with intrinsic p-type conductivity, ideal bandgap for visible light absorption ($\sim$1.6 eV) having superior light absorption coefficient ($>10^4\,cm^{-1}$), and high photo-responsivity (>0.1 A/W).[12–14] Owing to its multivalent nature, several stable 2D phases have been predicted theoretically,[15] but experimental realization of the same still remains a challenge. Fan *et al.* have used a liquid phase exfoliation method to

synthesize non-layered 2D Se nano-flakes from bulk selenium.[16] Though physical vapor transport (PVT) has been an established route for the synthesis of selenene, it lacks in crystallinity.[17] Also, chemical vapor transport (CVT) has been used for the growth of high-quality 2D materials. However, growing a large-sized, highly crystalline 2D Se with a controllable number of layers has been a great challenge till date. In our previous work,[11] we have been successful in synthesizing seeding-mediated CVT grown layered 2D triangular nano-flakes of crystalline t-Se. The application of 2D Se in the field of opto-electronics requires detailed knowledge of the excited carrier dynamics of the material. Femtosecond transient absorption/reflection (TA/TR) spectroscopy is a very mature technique used to monitor photo-induced excitation and relaxation processes by observing the change in absorbance/reflectance of a material before and after excitation.[18–22]

Multi-photon absorption (MPA) is a nonlinear optical process, where an electron gets excited to the conduction band by absorbing two or more photons simultaneously. Many research works have shown that 2D materials are susceptible to MPA.[23–28] One-photon absorption (OPA) mainly excites the surface region of the sample whereas MPA dominantly excites the sub-surface of the sample due to its higher penetration depth capability. There can be significant difference in the carrier dynamics of the surface and sub-surface region of the sample especially for 2D materials. Generally, the trap state density is noticeably higher in the surface region due the presence of dangling bonds drastically affecting the recombination dynamics.[29,30] Various techniques like Z scan,[31–33] TA/TR spectroscopy,[34–36] and multi-photon absorption photoluminescence saturation[37] are used to observe MPA processes.

Though detailed carrier dynamics of Se in bulk or QD form[12,38] has been discussed, comprehensive carrier dynamics study for 2D Se is still missing. This work comprehensively investigates the ultrafast carrier dynamics of 2D Se using our well established femtosecond TR/TA spectroscopy setup[39–46] in OPA and MPA regimes. Decay dynamics of the TR spectrum reflects dominance of trap state assisted charge carrier recombination. Pump wavelength dependent TR spectroscopy study shows the presence of MPA for 2D Se with a large two-photon absorption cross section. The excited carrier decay dynamics result shows one order longer decay constant for a three photon absorption regime compared to OPA. Our results provide deeper insight into the processes and timescales of carrier relaxation for 2D Se in OPA and MPA regimes, which are of outmost importance for their linear and non-linear opto-electronic applications.

We have synthesized 2D Se triangular nano-flakes on a Si/SiO_2 substrate using a metal seed mediated CVT method. The as-grown triangular shape of 2D Se nano-flakes is evident from the optical image [Fig. 1(a)]. A high-angle annular dark-field scanning transmission electron microscopy (HAADF-STEM) image [Figs. 1(b) and 1(c)] clearly reveals the atomically resolved lattice structure in the (0001) direction whereas the Raman spectrum [Fig. 1(d)] confirms the phase of 2D selenium to be trigonal. The optical properties of 2D Se as steady state absorption and emission spectra are shown in Figs. 1(e) and 1(f). The detailed synthesis procedure and structural characterization methods with their results are discussed in the supplementary material (S1).

We have obtained the linear reflection spectrum of 2D Se using a low-intensity, broadband (450–800 nm) super-continuum pulse, generated using nonlinear sapphire crystal with a laser pulse of 50 fs at

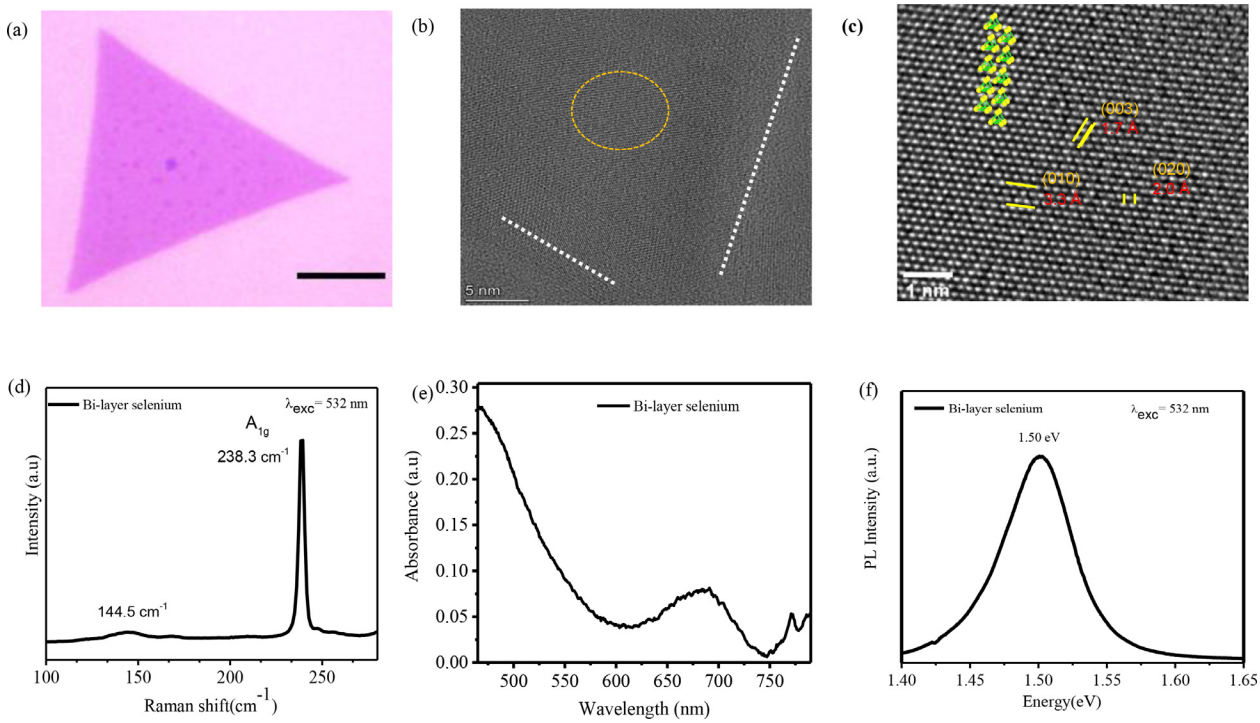

FIG. 1. (a) Optical image of 2D Se grown on the Si/SiO_2 substrate via the CVT method with Bi as the seed layer (the scale bar is 5 μm). (b) and (c) HAADF-STEM images of the 2D Se domain. The crystal structure is overlaid in the image with a ball-stick model. (d) Raman spectra of 2D Se and (e) calculated absorbance spectrum of 2D Se. (f) PL spectra recorded from 2D Se domains using a 532 nm pump.

800 nm. We first measured reflectivity of the SiO_2 substrate without (R_{sub}) and with (R_{Se}) 2D Se. Then we calculate a fractional change of reflectance of 2D Se and calculate absorbance of the sample [Fig. 1(e)] using the following equation:[47,48]

$$\delta R = \frac{R_{sub} - R_{Se}}{R_{sub}} = \frac{4}{n_s^2 - 1} A, \quad (1)$$

where n_s is the refractive index of the SiO_2 substrate and A is the absorbance of the selenium. Variation of differential reflectivity and refractive index of the substrate with probe wavelength is shown in the supplementary material (S2). The absorbance curve shows a peak around 700 nm (1.77 eV) for 2D Se. PL measurement [Fig. 1(f)] above the bandgap excitation wavelength of 532 nm shows a peak around 1.50 eV (826 nm) depicting the possibility of bandgap to be around 1.50 eV.

The electronic band structure of bilayer 2D Se has been calculated using the PBE (GGA) functional with Se_6-H as the most stable structure out of other 2D phases of Se confirmed by Sarma *et al.*[11] This is a 6-atom thick (bi-layer) structure with passivating terminals' Se atoms with hydrogen atoms in both the surfaces along the (001) direction [Fig. 2(a)].The calculated electronic band structure for the 2D bi-layer Se_6-H [Fig. 2(b)] shows the bandgap to be 1.70 eV.

Our measurements suggest that the bandgap of bi-layer Se is 1.50 eV, which breaks the underestimated principle of the GGA-PBE functional.[49] Therefore, there may be a possibility for trap state formation in between the bandgap and corresponding trap state transition from the band edges. As the 2D Se layer is passivated by H, the lightest element in the periodic table, hence there is a high chance to form the H-vacancy (V_H) in the system. The electronic band structure considering H-vacancy shows the bandgap of 1.68 eV [Fig. 2(d)]. The gap between the defect level and the conduction band minima is 1.23 eV depicting the lowest possible energy transition. The lowest energy transition for pristine and defect system is observed at 1.70 and 1.23 eV, respectively [Figs. 2(g) and 2(h)]. Detailed discussion is given in the supplementary material (S3).

To investigate ultrafast excited charge carrier dynamics, we performed femtosecond TR spectroscopy on 2D Se. This measurement is performed by measuring the difference of the probe reflection spectrum with and without pump excitation, providing transient reflection spectrum ΔR of 2D Se. The sign of change in reflection (ΔR) and change in absorption (ΔA) is the same for our study (supplementary material S5).

In TR spectroscopy, we use a 500 nm pump and visible (500–800 nm) and near IR (850–1100 nm) probe. The pump beam diameter and fluence are fixed at 2 mm and 64 $\mu J/cm^2$, respectively. In the visible probe region, the differential reflectivity spectrum [Figs. 3(a) and 3(b)] shows a broad positive reflectivity change ranging from 520 to 800 nm suggesting occurrence of excited state absorption (ESA) with two peaks around 585 (A) and 777 nm (B). We also observe a narrow bleaching like feature peaking around 790 nm (C) overlapped with the broad ESA background. The TR spectrum is quite similar with a monolithically integrated silicon light-emitting device (LED) in the wavelength range of 500–800 nm.[50] We observe broadband ESA in the near-IR probe region (900–1100 nm) shown in Figs. 3(e) and 3(f). The occurrence of ESA signal can mainly be the result of two possible nonlinear mechanisms: (i) bandgap renormalization (BGR) and (ii) free carrier absorption (FCA). The linear variation in the ESA amplitude with excited carrier density/pump fluence (Figs. S8 and S9) infers dominance of FCA in the occurrence of ESA.[51] The decay dynamics at various visible and near-IR probe wavelengths [Figs. 3(c) and 3(g)] are fitted with the tri-exponential decay function given below:[47]

$$\Delta A = A\left[-\exp\left(-\frac{t}{\tau_1}\right) + \sum_{i=2}^{3} A_i \exp\left(-\frac{t}{\tau_i}\right)\right], \quad (2)$$

where A is the maximum value of ΔA, τ_1 is the rise time constant, and τ_i and A_i are decay time constants (for i = 2 and 3) and their corresponding amplitudes, respectively. The obtained rise and decay time constants show the whole broad ESA region following similar decay dynamics (Table I). The rise time is correlated with the thermalization and average carrier cooling time. The carrier cooling time at all the concerned visible and near IR probe wavelengths are nearly the same (0.4–0.7ps) at 64 $\mu J/cm^2$ pump fluence (Table I). The fast and long

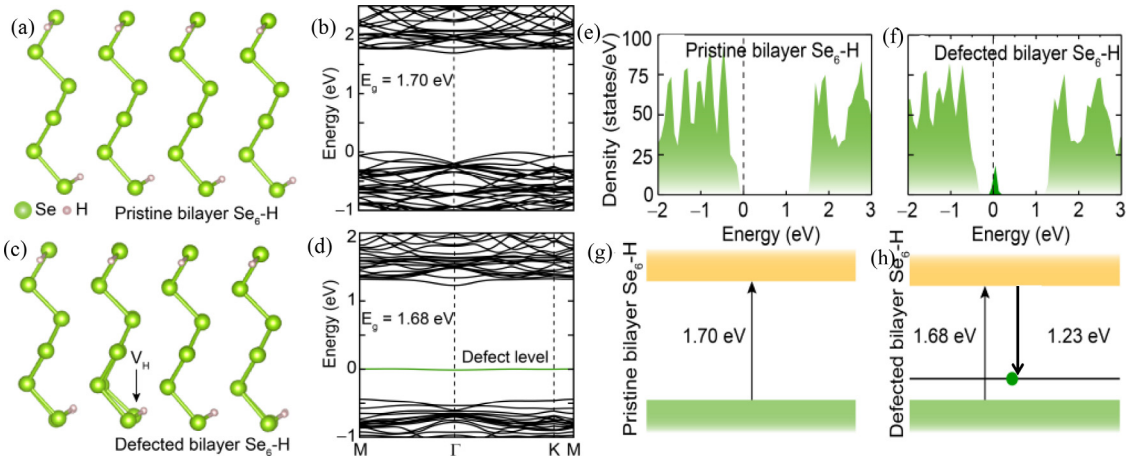

FIG. 2. (a) The optimized bilayer pristine structure of Se_6-H. (b) The electronic band structure of bilayer Se_6-H. (c) The optimized bilayer V_H defected structure of Se_6-H. (d) The electronic band structure of bilayer V_H-Se_6-H. (e) The density of states of bilayer Se_6-H. (f) The density of states of bilayer V_H-Se_6-H. (g) The lowest energy electronic transition schematic of Se_6-H. (h) The lowest energy electronic transition schematic of V_H-Se_6-H.

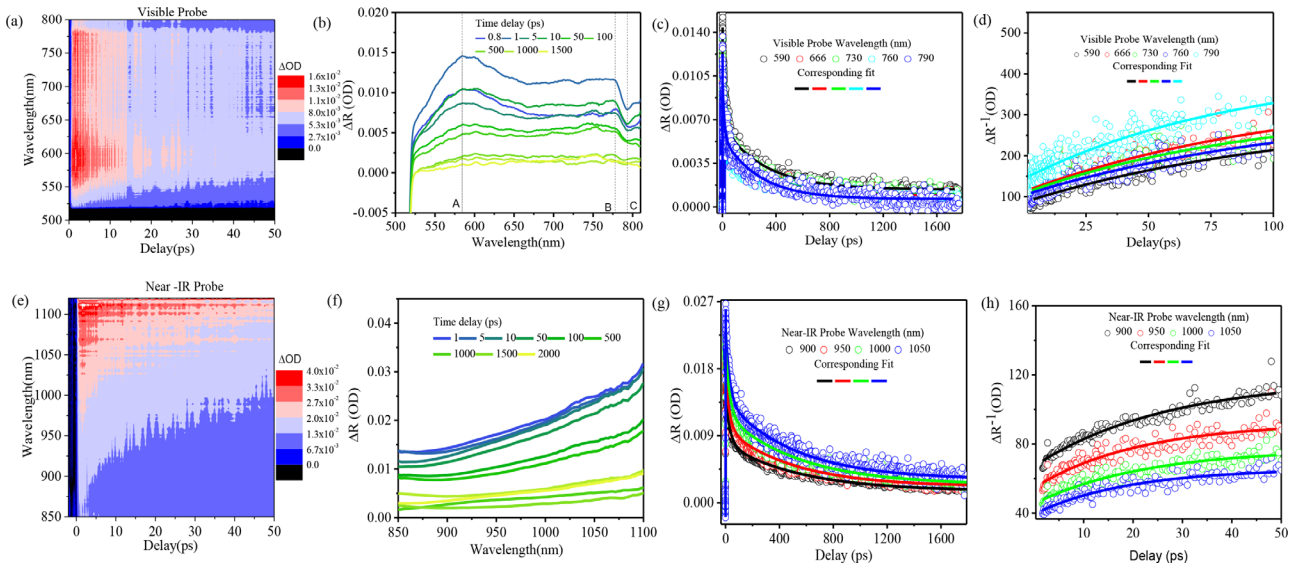

FIG. 3. (a) Contour plot and (b) corresponding TR spectrum at different time delay (ps) for 2D Se at visible probe wavelengths. The dotted lines are showing an excited absorption peak. (c) The fs-transient bleach decay kinetics with corresponding tri-exponential decay fits and (d) temporal variation of ΔR^{-1} at various visible probe wavelengths with their exponential fit. (e) Contour plot and (f) corresponding TR spectrum at different time delay (ps) for 2D Se at near-IR probe wavelengths. (g) The fs-transient bleach decay kinetics with corresponding tri-exponential decay fits and (h) temporal variation of ΔR^{-1} at various near-IR probe wavelengths with their exponential fit. All the above measurements are performed at a pump excitation of 500 nm with the fluence of 64 $\mu J/cm^2$.

decay times are nearly 14–20 and 270–320 ps, respectively, in the visible region whereas 30–33 and 515–550 ps in the near-IR region, respectively.

Recombination causes decay in the ESA amplitude. To understand the dominant recombination process, we have plotted temporal variation of ΔR^{-1} at various visible and near IR probe wavelengths [Figs. 3(d) and 3(h)]. It follows exponential variation at all probe wavelengths revealing the dominance of trap state assisted recombination.[45] The presence of defects in 2D materials is quite natural due to its growth process, high surface to volume ratio, and dangling bonds.[52,53] We have assigned the faster (τ_2) and slower decay constant (τ_3) to the surface and sub-surface recombination, respectively.

Pump fluence dependent kinetics is fitted with Eq. (2) (Figs. S10 and S12). Fluence invariant rise time (τ_1) indicates the absence of hot phonon bottleneck effect in 2D Se (Fig. S14). Reduction of decay constants (τ_2 and τ_3) with increased pump fluence (13–79 $\mu J/cm^2$) depicts faster recombination (Figs. S11 and S13). The carrier lifetimes are in the same order with various mono- and few-layer TMDs who have great photo-detector application.[54–56]

We identify one-photon (380–650 nm), two-photon (700–800 nm), and three-photon (900–1200 nm) absorption regimes [Fig. 4(b)] for 2D Se by pump-wavelength dependent TR measurement (supplementary material S11). The average pump power used in three-photon excitation is nearly three orders of magnitude higher than one-photon excitations (0.2 mW for 380 nm and 100 mW for 1200 nm) to get similar ESA amplitude (~6 mOD) [Fig. 4(b)]. We need very high optical power for MPA due to low transition probability and weak absorption coefficient/cross section of MPA with respect to OPA. Wei *et al.* have shown that the 2PA absorption coefficient of $MAPbCl_3$ at 800 nm is 1.8 $\times 10^{-3}$ cm GW^{-1}, whereas the 3PA absorption coefficient is 1.3 $\times$ 10^{-7} cm^3GW^{-2}.[57] Pramanik *et al.* have shown that values of 1PA, 2PA, and 3PA cross sections of $CsPbBr_3$ are 9.3 $\times$ 10^{-14} cm^2, 1.8 $\times$ 10^{-45} cm^4 s^{-1}photon^{-1}, and 3.1 $\times$ 10^{-75} cm^6s^{-2}photon^{-2}, respectively.[58]

TABLE I. Decay time constants of 2D Se determined by fitting ESA dynamics with a tri-exponential decay function [Eq. (2)] at various probe wavelengths.

Probe wavelength (nm) (visible region)	τ_1 (ps)	τ_2 (ps)	τ_3 (ps)	Probe wavelength (nm) (near IR region)	τ_1 (ps)	τ_2 (ps)	τ_3 (ps)
790	0.6 ± 0.05	14 ± 1	275 ± 20	900	0.37 ± 0.01	33.4 ± 2	550.3 ± 15
760	0.78 ± 0.1	13.2 ± 1	270.5 ± 20	950	0.37 ± 0.1	30.7 ± 3	512 ± 12
730	0.5 ± 0.15	14 ± 1	287 ± 23	1000	0.39 ± 0.15	32 ± 1	546 ± 20
666	0.4 ± 0.1	19 ± 2	289 ± 23	1050	0.4 ± 0.1	29.4 ± 1	515 ± 25
590	0.5 ± 0.14	22 ± 2	317 ± 24				

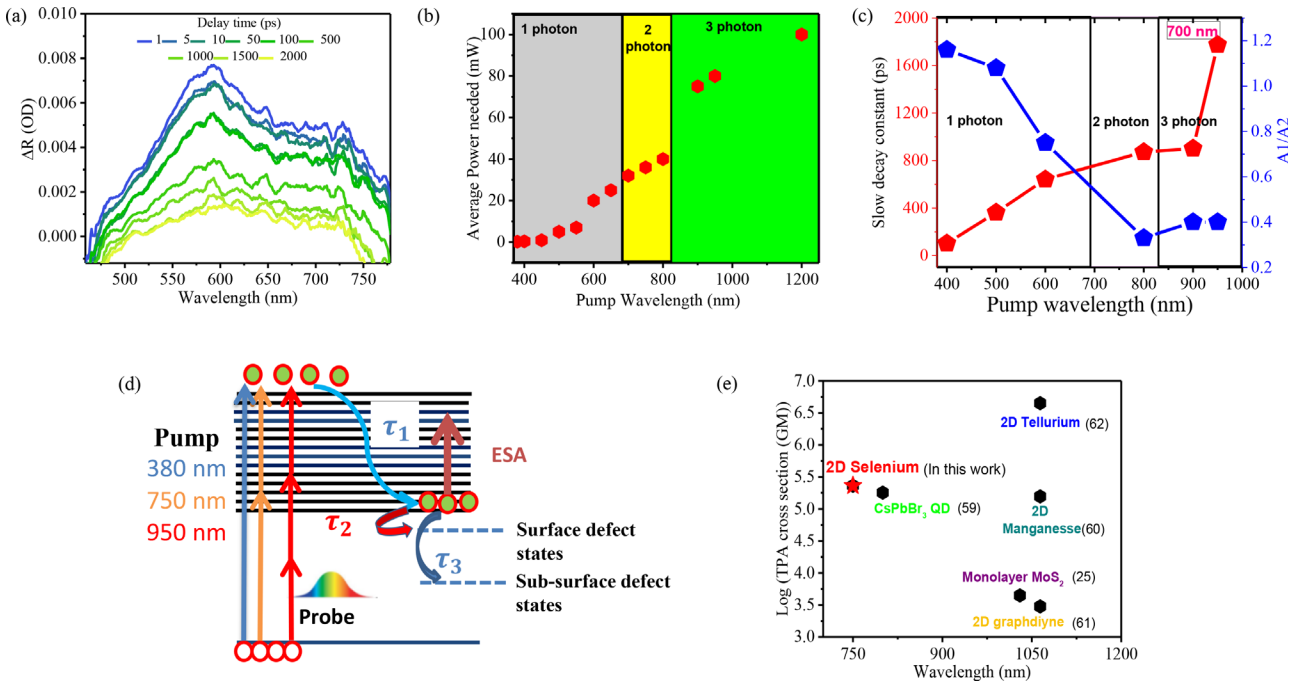

FIG. 4. (a) TR spectrum of 2D Se at different time delay (ps) under the excitation of 950 nm pump having a fluence of 1272 μJ/cm^2. (b) Variation in average pump power needed for having the same ESA amplitude (6 mOD) at various pump photon wavelengths with one and multi-photon absorption regimes assigned. (c) Variation of slow decay constant (τ_3) and amplitude ratio (A_2/A_3) of corresponding exponential decay constants with pump photon wavelength. (d) Model diagram to understand single and multi-photon carrier generation and recombination of 2D Se. (e) Comparison of the TPA cross section of 2D Se with other 2D materials.

We have calculated OPA and two-photon absorption (TPA) cross sections from our steady state absorption and TR measurement using the following equations:[34]

$$\Delta A_{ESA} = \frac{(1-10^{-A})}{ln10} J_P \sigma^{(1)} \tag{3}$$

and

$$\Delta A^{(2)}_{ESA} = A.\frac{J_p^2}{2\tau_p}\sigma^{(2)}, \tag{4}$$

where ΔA_{ESA}, $\Delta A^{(2)}_{ESA}$, A, J_P, $\sigma^{(1)}$, $\sigma^{(2)}$, and τ_p are the ESA amplitude at OPA and TPA regimes, absorbance at the pump wavelength, the surface density of pump photons, OPA and TPA cross sections, and pulse duration, respectively. The calculated values of OPA and TPA cross sections are 15.3×10^{-16}cm^2 at 450 nm and 2.9×10^5 GM at 750 nm, respectively (supplementary material S12). The dominance of the TPA cross section in 2D Se with respect to other conventional 2D semiconductors[25,59–62] is shown in Fig. 4(e). The presence of large TPA cross section is due to the strong electronic confinement in 2D Se,[63] which creates the possibility of 2D Se to be used as the sub-bandgap photo-detector.[64–66]

We have investigated carrier dynamics in OPA and MPA regimes. For 380 nm pump wavelength, the decay dynamics is fitted by a bi-exponential decay function, whereas for higher pump wavelength, it has been fitted by a tri-exponential decay function (supplementary material S13). The fitted decay constants (τ_2 and τ_3) with the ratio of corresponding amplitude (A_2 and A_3) are tabulated in Table II. Slow decay constant (τ_3) increases with an increase in the pump wavelength [103 ps at 400 nm (one-photon regime) and 1700 ps at 950 nm (three-photon regimes)]. We propose a generalized model to explain excited carrier dynamics in different pumping regimes [Fig. 4(d)]. Unlike OPA, more than one photon is needed to excite the electron from a valence band to a higher conduction band in the MPA regime. The excited electrons cool down to the conduction band minima and then get probe-excited. The cooling of the excited carriers is denoted by τ_1, which remains nearly constant in all pumping regimes. The faster (τ_2) and slower decay constant (τ_3) have been correlated with surface and sub-surface trap-assisted recombination, respectively. One-photon and multi-photon excitation mainly excites

TABLE II. Pump-wavelength dependent fast and slow decay constants with ratio of their respective amplitudes.

Pump wavelength (nm)	A_2	τ_2 (ps)	A_3	τ_3 (ps)	A_2/A_3
380	0.89	2.3	...	...	...
400	0.5	6	0.3	103	1.66
500	0.4	12	0.4	363	1
800	0.3	17.4	0.45	872	0.66
900	0.2	13	0.4	902	0.5
950	0.19	12	0.34	1700	0.55

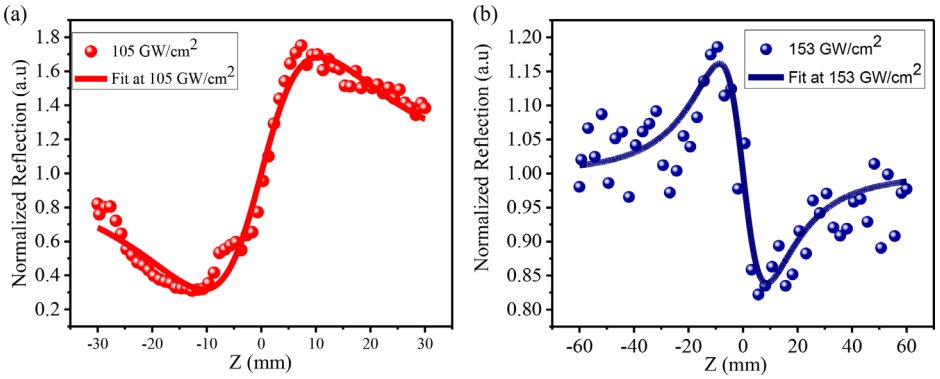

FIG. 5. Close aperture reflection Z scan at (a) 500 nm with a pump intensity of 105 GW/cm^2 and (b) 1000 nm with 153 GW/cm^2 on 2D Se.

the carriers from the top layer and the depth of the sample, respectively.[27] Larger trap state density in the surface results higher recombination and lower carrier lifetime.[67] Slow decay constant (τ_3) increases by two orders of magnitude when it changes from one-photon to three-photon pumping regimes. In the case of lowest pump wavelength (380 nm), the decay of the ESA signal is governed by a single decay pathway (τ_2, surface recombination), but as the pump wavelength increases, a new pathway (τ_3, sub-surface recombination) appears. We observe the dominance of sub-surface recombination over surface recombination as their amplitude ratio (A_2/A_3) decreases in the MPA regime (Table II).

We have theoretically calculated the responsivity of the photodetector based on 2D Se using our TR results. Here, the photoresponsivity (R^*) is defined as

$$R^* = \frac{I_{ph}}{P_{in}} * G, \tag{5}$$

where I_{ph} is the generated photo-current corresponding to incident optical power, P_{in} and G is the photo-conductive gain given by

$$G = \frac{\tau_r}{\tau_l}, \tag{6}$$

where τ_r is the carrier lifetime and τ_l is the carrier transit time. Using Eqs. (5) and (6), we have calculated the value of R^* about 7.78 μA/W for 500 nm excitation with an average power of 5mW (supplementary material S14).

We perform reflection close aperture (R-CA) Z-scan[68] at the excitation wavelengths 500 nm (2.48 eV) and 1000 nm (1.24 eV) on 2D Se. The normalized reflection data show the valley-peak configurations at 500 nm beam excitation, indicating saturable absorption (SA) of the material [Fig. 5(a)]. The SA coefficient (α) at 500 nm is $\alpha = -(1.2403 \pm 0.0276) \times 10^3$ cm/GW at 105 GW/cm^2 excitation. The z-scan result shows a change from valley to peak in between the sample position −10 to 10 mm. Since R-CA measurement at 500 nm (∼2.48 eV) is taken above the bandgap (∼1.5 eV), we can predict the band saturation occurs due to one photon absorption. At below the bandgap excitation (1000 nm), 2D Se shows a peak-valley configuration [Fig. 5(b)] showing the presence of reverse saturable absorption (RSA). The z-scan result shows a change from peak to value in between the sample position −15 and 20 mm. This RSA property arises due to TPA. The TPA coefficient (β) at peak intensity 153 GW/cm^2 is $\beta = (69.4811 \pm 2.0900)$ cm/GW, which is of the order of atomically thin layered TMDS like MoS_2.[69] The nonlinear properties of the material suggest that bi-layer Se can be used as a saturable absorber for passive Q-switching and mode-locking in the visible region.[70] The intensity variation nonlinear absorption coefficients are tabulated in Table S3. The experimental details and related theoretical formulas are summarized in supplementary section S15.

In conclusion, we have investigated ultrafast carrier dynamics of 2D Se revealing a trap state dominated recombination process using TR spectroscopy. Carrier lifetime obtained from TR measurement is used to theoretically predict the photo-responsivity for the 2D Se photo-detector operating in the OPA regime. We have observed the presence of MPA with strikingly high TPA cross sections of 2.3×10^5 GM. Pump wavelength dependent TR measurement probing surface and sub-surface kinetics show one order faster recombination for OPA compared to MPA due to the presence of higher defect state density in the surface region. Defect assisted recombination of a sub-surface dominates over surface recombination in the MPA regime. Z-scan measurement results show SA and RSA nature of 2D Se in above and below bandgap excitation, respectively. This shows dominance of TPA in below bandgap excitation. Direct bandgap nature, high carrier lifetime, and the presence of MPA show the great possibility of 2D Se to be used as above- and sub-bandgap photodetectors. This work unravels basic understanding about the trap state dominated ultrafast carrier dynamics probing surface and subsurface kinetics of 2D Se in one and multi-photon absorption regimes and provides the platform to study modulation of carrier lifetime to have great potential in linear and non-linear ultrathin optoelectronic devices.

See the supplementary material for detailed methods of synthesis and structural characterization of two dimensional selenium and discussion on their result, variation of differential reflectivity and substrate refractive index, detailed discussion on the DFT method and its result, schematic setup of transient reflection spectroscopy, relation between a change in reflection and a change in absorption, variation in the PIA amplitude with pump fluence variation for visible probe, variation in the PIA amplitude with pump fluence variation for IR probe, variation of fitted decay constants with pump fluence variation for visible probe, hot carrier cooling time with pump wavelength variation, determination of one and multi-photon absorption regimes, determination of OPA and MPA cross section, theoretical calculation of photo-detector responsivity, and reflection Z-scan.

This work was supported by the equipment grant of UPM (SGDRI) Project of IIT Kharagpur. The author Sayan Prodhan acknowledges UGC, Government of India for research fellowship.

AUTHOR DECLARATIONS

Conflict of Interest

The authors have no conflicts to disclose.

Author Contributions

Sayan Prodhan: Conceptualization (lead); Data curation (lead); Formal analysis (lead); Investigation (lead); Methodology (lead); Writing – original draft (lead); Writing – review & editing (lead). **M. Shaijumon:** Supervision (equal); Writing – review & editing (supporting). **Prasanta Kumar Datta:** Conceptualization (equal); Methodology (equal); Supervision (lead); Writing – review & editing (equal). **Kamlesh Kumar Chauhan:** Conceptualization (equal); Writing – review & editing (equal). **Tara Singha:** Investigation (equal); Writing – review & editing (supporting). **Manobina Karmakar:** Conceptualization (equal); Formal analysis (equal); Writing – review & editing (equal). **Nikhilesh Maity:** Formal analysis (equal); Investigation (equal); Software (lead). **Renjith Nadarajan:** Formal analysis (equal); Investigation (equal). **Partha Kumbhakar:** Writing – review & editing (supporting). **Chandra sekhar Tiwary:** Supervision (equal); Writing – review & editing (supporting). **Abhishek Kumar Singh:** Supervision (equal); Writing – review & editing (supporting).

DATA AVAILABILITY

The data that support the findings of this study are available within the article and its supplementary material.

REFERENCES

[1]K. S. Novoselov, A. K. Geim, S. V. Morozov, D. Jiang, Y. Zhang, S. V. Dubonos, I. V. Grigorieva, and A. A. Firsov, Science **306**, 666 (2004).
[2]A. J. Mannix, B. Kiraly, M. C. Hersam, and N. P. Guisinger, Nat. Rev. Chem. **1**, 0014 (2017).
[3]N. R. Glavin, R. Rao, V. Varshney, E. Bianco, A. Apte, A. Roy, E. Ringe, and P. M. Ajayan, Adv. Mater. **32**, 1904302 (2020).
[4]Q. Ma, G. Ren, K. Xu, and J. Z. Ou, Adv. Opt. Mater. **9**, 2001313 (2021).
[5]Z. Lin, C. Wang, and Y. Chai, Small **16**, 2002426 (2020).
[6]Z. Shi, R. Cao, K. Khan, A. K. Tareen, X. Liu, W. Liang, Y. Zhang, C. Ma, Z. Guo, X. Luo, and H. Zhang, Nano-Micro Lett. **12**, 99 (2020).
[7]D. K. Sang, B. Wen, S. Gao, Y. Zeng, F. Meng, Z. Guo, and H. Zhang, Nanomaterials **9**, 1075 (2019).
[8]Z. Yan, H. Yang, Z. Yang, C. Ji, G. Zhang, Y. Tu, G. Du, S. Cai, and S. Lin, Small **18**, 2200016 (2022).
[9]Y. Wang, G. Qiu, R. Wang, S. Huang, Q. Wang, Y. Liu, Y. Du, W. A. Goddard, M. J. Kim, X. Xu, P. D. Ye, and W. Wu, Nat. Electron. **1**, 228 (2018).
[10]C. Xing, Z. Xie, Z. Liang, W. Liang, T. Fan, J. S. Ponraj, S. C. Dhanabalan, D. Fan, and H. Zhang, Adv. Opt. Mater. **5**, 1700884 (2017).
[11]P. V. Sarma, R. Nadarajan, R. Kumar, R. M. Patinharayil, N. Biju, S. Narayanan, G. Gao, C. S. Tiwary, M. Thalakulam, R. N. Kini, A. K. Singh, P. M. Ajayan, and M. M. Shaijumon, 2D Mater. **9**, 045004 (2022).
[12]M. Zhu, F. Hao, L. Ma, T. B. Song, C. E. Miller, M. R. Wasielewski, X. Li, and M. G. Kanatzidis, ACS Energy Lett. **1**, 469 (2016).
[13]D. Wang, L. M. Tang, X. X. Jiang, J. Y. Tan, M. D. He, X. J. Wang, and K. Q. Chen, Adv. Electron. Mater. **5**, 1800475 (2019).
[14]J. K. Qin, G. Qiu, W. He, J. Jian, M. W. Si, Y. Q. Duan, A. Charnas, D. Y. Zemlyanov, H. Y. Wang, W. Z. Shao, L. Zhen, C. Y. Xu, and P. D. Ye, Adv. Funct. Mater. **28**, 1806254 (2018).
[15]C. Liu, T. Hu, Y. Wu, H. Gao, Y. Yang, and W. Ren, J. Phys. Condens. Matter **31**, 235702 (2019).
[16]T. Fan, Z. Xie, W. Huang, Z. Li, and H. Zhang, Nanotechnology **30**, 114002 (2019).
[17]J. Qin, G. Qiu, J. Jian, H. Zhou, L. Yang, A. Charnas, D. Y. Zemlyanov, C. Y. Xu, X. Xu, W. Wu, H. Wang, and P. D. Ye, ACS Nano **11**, 10222 (2017).
[18]W. Wang, N. Sui, Z. Kang, Q. Zhou, L. Li, X. Chi, H. Zhang, X. He, B. Zhao, and Y. Wang, Opt. Express **29**, 7736 (2021).
[19]J. Fu, Q. Xu, G. Han, B. Wu, C. H. A. Huan, M. L. Leek, and T. C. Sum, Nat. Commun. **8**, 1300 (2017).
[20]C. E. Petoukhoff, S. Kosar, M. Goto, I. Bozkurt, M. Manish, and K. M. Dani, Mol. Syst. Des. Eng. **4**, 929 (2019).
[21]J. Cho, J. T. DuBose, and P. V. Kamat, J. Phys. Chem. Lett. **11**, 2570 (2020).
[22]C. M. Wolff, S. A. Bourelle, L. Q. Phuong, J. Kurpiers, S. Feldmann, P. Caprioglio, J. A. Marquez, J. Wolansky, T. Unold, M. Stolterfoht, S. Shoaee, F. Deschler, and D. Neher, Adv. Energy Mater. **11**, 2101823 (2021).
[23]H. Yang, X. Feng, Q. Wang, H. Huang, W. Chen, A. T. S. Wee, and W. Ji, Nano Lett. **11**, 2622 (2011).
[24]S. Zhang, N. Dong, N. McEvoy, M. O'Brien, S. Winters, N. C. Berner, C. Yim, Y. Li, X. Zhang, Z. Chen, L. Zhang, G. S. Duesberg, and J. Wang, ACS Nano **9**, 7142 (2015).
[25]Y. Li, N. Dong, S. Zhang, X. Zhang, Y. Feng, K. Wang, L. Zhang, and J. Wang, Laser Photonics Rev. **9**, 427 (2015).
[26]W. Liu, J. Xing, J. Zhao, X. Wen, K. Wang, P. Lu, and Q. Xiong, Adv. Opt. Mater. **5**, 1601045 (2017).
[27]J. Wang, Y. Mi, X. Gao, J. Li, J. Li, S. Lan, C. Fang, H. Shen, X. Wen, R. Chen, X. Liu, T. He, and D. Li, Adv. Opt. Mater. **7**, 1900398 (2019).
[28]F. Zhou, I. Abdelwahab, K. Leng, K. P. Loh, and W. Ji, Adv. Mater. **31**, 1904155 (2019).
[29]B. Wu, H. T. Nguyen, Z. Ku, G. Han, D. Giovanni, N. Mathews, H. J. Fan, and T. C. Sum, Adv. Energy Mater. **6**, 1600551 (2016).
[30]K. Xu, J. Opt. **20**, 024014 (2018).
[31]J. Olesiak-Banska, M. Waszkielewicz, K. Matczyszyn, and M. Samoc, RSC Adv. **6**, 98748 (2016).
[32]A. Gaur, H. Syed, B. Yendeti, and V. R. Soma, J. Opt. Soc. Am. B **35**, 2906 (2018).
[33]S. K. Patra, B. K. Dadhich, B. Bhushan, R. K. Choubey, and A. Priyam, ACS Omega **6**, 31375 (2021).
[34]J. Moreno, A. L. Dobryakov, I. N. Ioffe, A. A. Granovsky, S. Hecht, and S. A. Kovalenko, J. Chem. Phys. **143**, 024311 (2015).
[35]Y. D. Glinka, T. He, and X. W. Sun, J. Phys.: Condens. Matter **34**, 465301 (2022).
[36]A. Iagatti, B. Shao, A. Credi, B. Ventura, I. Aprahamian, and M. Di Donato, Beilstein J. Org. Chem. **15**, 2438 (2019).
[37]A. Alo, L. W. T. Barros, G. Nagamine, L. B. Vieira, J. H. Chang, B. G. Jeong, W. K. Bae, and L. A. Padilha, ACS Photonics **7**, 1806 (2020).
[38]X. Jiang, W. Huang, R. Wang, H. Li, X. Xia, X. Zhao, L. Hu, T. Chen, Y. Tang, and H. Zhang, Nanoscale **12**, 11232 (2020).
[39]K. K. Chauhan, S. Prodhan, D. Ghosh, P. Waghale, S. Bhattacharyya, P. K. Dutta, and P. K. Datta, IEEE J. Photovoltaics **10**, 803 (2020).
[40]A. Ghosh, D. K. Chaudhary, A. Mandal, S. Prodhan, K. K. Chauhan, S. Vihari, G. Gupta, P. K. Datta, and S. Bhattacharyya, J. Phys. Chem. Lett. **11**, 591 (2020).
[41]S. Bhattacharya, A. Ghorai, S. Raval, M. Karmakar, A. Midya, S. K. Ray, and P. K. Datta, Carbon N. Y. **134**, 80 (2018).
[42]M. Karmakar, S. Bhattacharya, S. Mukherjee, B. Ghosh, R. K. Chowdhury, A. Agarwal, S. K. Ray, D. Chanda, and P. K. Datta, Phys. Rev. B **103**, 075437 (2021).
[43]M. Karmakar, S. Mukherjee, S. K. Ray, and P. K. Datta, Phys. Rev. B **104**, 075446 (2021).
[44]K. K. Chauhan, S. Prodhan, S. Bhattacharyya, P. K. Dutta, and P. K. Datta, IEEE J. Quantum Electron. **57**, 4800108 (2020).
[45]S. Prodhan, K. K. Chauhan, M. Karmakar, A. Ghosh, S. Bhattacharyya, and P. K. Datta, J. Phys. D: Appl. Phys. **55**, 014002 (2022).
[46]M. Karmakar, P. Kumbhakar, T. Singha, C. S. Tiwary, D. Chanda, and P. K. Datta, Phys. Rev. B **107**, 075429 (2023).
[47]K. F. Mak, M. Y. Sfeir, Y. Wu, C. H. Lui, J. A. Misewich, and T. F. Heinz, Phys. Rev. Lett. **101**, 196405 (2008).
[48]L. Gao, R. Lemarchand, and M. Lequime, J. Eur. Opt. Soc. **8**, 13010 (2013).

[49]J. P. Perdew, Int. J. Quantum Chem. **28**, 497 (2009).
[50]K. Xu, J. Micromech. Microeng. **31**, 054001 (2021).
[51]Y. Yang, D. P. Ostrowski, R. M. France, K. Zhu, J. van de Lagemaat, J. M. Luther, and M. C. Beard, Nat. Photonics **10**, 53 (2016).
[52]M. L. Benkhedir, M. S. Aida, and G. J. Adriaenssens, J. Non. Cryst. Solids **344**, 193 (2004).
[53]S. Imura, K. Mineo, K. Miyakawa, M. Kubota, and M. Nanba, Appl. Phys. Lett. **116**, 252103 (2020).
[54]H. Shi, R. Yan, S. Bertolazzi, J. Brivio, B. Gao, A. Kis, D. Jena, H. G. Xing, and L. Huang, ACS Nano **7**, 1072 (2013).
[55]S. H. Aleithan, M. Y. Livshits, S. Khadka, J. J. Rack, M. E. Kordesch, and E. Stinaff, Phys. Rev. B **94**, 035445 (2016).
[56]C. Ruppert, A. Chernikov, H. M. Hill, A. F. Rigosi, and T. F. Heinz, Nano Lett. **17**, 644 (2017).
[57]K. H. Wei, B. J. Chen, L. B. Zhang, H. R. Zhu, and S. H. Fan, Laser Phys. Lett. **19**, 056003 (2022).
[58]A. Pramanik, K. Gates, Y. Gao, S. Begum, and P. Chandra Ray, J. Phys. Chem. C **123**, 5150 (2019).
[59]J. Chen, K. Žídek, P. Chábera, D. Liu, P. Cheng, L. Nuuttila, M. J. Al-Marri, H. Lehtivuori, M. E. Messing, K. Han, K. Zheng, and T. Pullerits, J. Phys. Chem. Lett. **8**, 2316 (2017).
[60]Y. Xin, J. Yuan, Y. Liu, Z. Zhao, B. Du, F. Xing, and F. Zhang, ACS Appl. Nano Mater. **5**, 8080 (2022).
[61]F. Zhang, G. Liu, J. Yuan, Z. Wang, T. Tang, S. Fu, H. Zhang, Z. Man, F. Xing, and X. Xu, Nanoscale **12**, 6243 (2020).
[62]F. Zhang, G. Liu, Z. Wang, T. Tang, X. Wang, C. Wang, S. Fu, F. Xing, K. Han, and X. Xu, Nanoscale **11**, 17058 (2019).
[63]R. Scott, A. W. Achtstein, A. Prudnikau, A. Antanovich, S. Christodoulou, I. Moreels, M. Artemyev, and U. Woggon, Nano Lett. **15**, 4985 (2015).
[64]G. Walters, B. R. Sutherland, S. Hoogland, D. Shi, R. Comin, D. P. Sellan, O. M. Bakr, and E. H. Sargent, ACS Nano **9**, 9340 (2015).
[65]M. Adnan and G. V. Prakash, J. Phys. Chem. C **125**, 12166 (2021).
[66]D. Dini, R. Köhler, A. Tredicucci, G. Biasiol, and L. Sorba, Phys. Rev. Lett. **90**, 116401 (2003).
[67]H. Wang, C. Zhang, and F. Rana, Nano Lett. **15**, 8204 (2015).
[68]X. Huang, X. H. Zhang, Y. G. Zhu, T. Li, L. F. Han, X. J. Shang, H. Q. Ni, and Z. C. Niu, Opt. Commun. **283**, 1510 (2010).
[69]M. E. Maldonado, A. Das, A. M. Jawaid, A. J. Ritter, R. A. Vaia, D. A. Nagaoka, P. G. Vianna, L. Seixas, C. J. S. de Matos, A. Baev, P. N. Prasad, and A. S. L. Gomes, ACS Photonics **7**, 3440 (2020).
[70]T. Singha, M. Karmakar, P. Kumbhakar, C. S. Tiwary, and P. K. Datta, Appl. Phys. Lett. **120**, 021101 (2022).